

Substorm onsets as observed by IMAGE-FUV

H. U. Frey and S. B. Mende

Abstract: The FUV instrument observed more than 4000 substorm onsets during the 5.5 years of the IMAGE mission. About 2/3 were observed during the first 3 years in the northern hemisphere, while 1/3 were observed towards the end of the mission in the southern hemisphere. The locations of individual substorms are influenced by the external solar wind conditions, primarily the B_y and B_z components of the IMF. However, when averaged over all seasons and several years, the average substorm onset locations are the same in both hemispheres with respect to magnetic latitude and local time. This result signifies that the source region of substorms and the final onset location in the ionosphere, are primarily determined by the internal properties of the magnetosphere, and only secondarily influenced by external conditions.

Key words: Substorms, onset location, hemispheres.

1. Introduction

Substorms are one of the most outstanding signatures of the coupling between the magnetosphere and the ionosphere. They suddenly release hundreds of GW of power in the magnetotail, create intense plasma flows in the plasma sheet, build up strong field-aligned currents, excite almost all kinds of electromagnetic waves, and cause strong energetic particle precipitation that create bright and dynamic auroras in the ionosphere. Their temporal development is reasonably well described by the traditional picture of growth, onset, expansion, and recovery phases [1, 16]. What is still the topic of intense discussion are the exact temporal development of the single phases, the locations of phenomena in the magnetosphere, and the conjugacy of the auroral breakup. Two substorm theories propose different onset locations and sequences of events. The Current Disruption Model puts the onset location near Earth ($< 8R_e$) with a current disruption that is quickly followed by the auroral breakup [14, 2]. The Near-Earth Neutral Line Model [9] places the substorm initiation at $\approx 15 - 25R_e$ and the auroral breakup occurs later than in the Current Disruption Model when the fast flows break near the earth [22].

The first extensive study of seasonal and interplanetary magnetic field (IMF) effects on substorm onsets used 648 Polar UVI northern hemisphere observations in 1996-1997 shortly after the minimum of the past solar cycle [11]. The authors found systematic changes of lower onset latitude for $B_x > 0$ or $B_z < 0$ and increased latitudes for $B_x < 0$ or $B_z > 0$, respectively. The onset longitude depends on season and IMF B_y . In summer, substorms tend to occur in the early evening, whereas in winter they tend to occur near midnight with an average difference of ≈ 1 hour of MLT. Onset locations also shift toward earlier local times for $B_y > 0$ and toward midnight for $B_y < 0$. The authors also concluded that substorm onsets should not be conjugate.

This conclusion was confirmed in 2001 and 2002, when the Imager for Magnetopause-to-Aurora Global Exploration (IMAGE) satellite had its apogee in the Northern Hemisphere and the Polar spacecraft, owing to the apsidal precession of its or-

bit, reached higher altitudes in the Southern Hemisphere [19]. The two spacecraft offered a unique opportunity to study the aurora in the conjugate hemispheres simultaneously. Five substorm onsets were compared in the two hemispheres, which had asymmetric locations. The longitudinal displacement in one hemisphere compared with the other can be as much as 1.5 hours of local time. For southward IMF the hemispherical asymmetry in local time is strongly correlated with the IMF clock angle. These findings were interpreted as the magnetic tensions force acting on open magnetic field lines before reconnecting in the magnetotail. A similar asymmetry of substorms was found with SuperDARN radars [20]. Systematic asymmetries in the interhemispheric signatures of the auroral westward flow channels probably arose because the magnetic flux tubes were distorted at L shells passing close to the substorm dipolarisation region.

The FUV imager on the IMAGE spacecraft observed the northern hemisphere aurora between 2000 and 2002. Small subsets of its images were used to compare the behavior of the proton and electron aurora during the substorm expansion. The analysis of 78 winter substorms did not find any significant difference in the spatial distribution of the proton and electron onsets [6]. However, they found a strong anti-correlation between the onset latitude and the one-hour averaged solar wind dynamic pressure before the onset. The analysis of 91 substorms established that there are differences in the expansion of the electron and proton precipitation after onset [18]. The investigation of the high-latitude ionospheric flow during 67 substorms demonstrated the increase of the dawn-to-dusk transpolar voltage during the first minutes after substorm onset [21].

A much more extensive investigation determined all substorm onsets that were observed in the northern hemisphere by IMAGE-FUV between May 2000 and December 31, 2002 [5]. A total of 2437 substorms were found and their average onset location was 2300 hours MLT and 66.4° magnetic latitude. These values agreed reasonably well with previous reports though such investigations used smaller numbers of substorms and/or were limited to certain seasons [3, 7, 11, 6]. The published list of substorm onsets has so far been used in one published paper that investigated the location of auroral breakups in response to solar illumination and solar coupling parameters [24]. It was found that solar illumination and the related ionospheric conductivity have significant effects on the most

Received 10 May 2006.

H. U. Frey and S. B. Mende. University of California, Space Sciences Laboratory, Berkeley, CA 94720, USA.

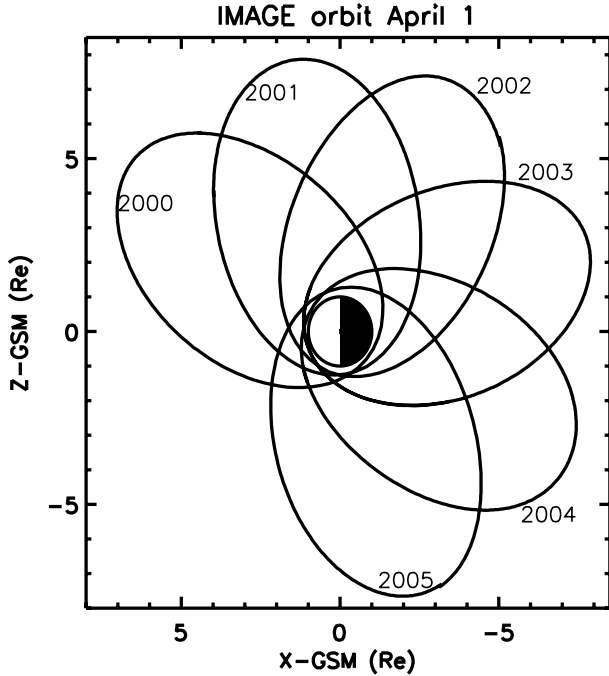


Fig. 1. Change of the IMAGE orbit from launch in 2000 until 2005. The orbit is shown for April 1st each year when the orbital plane was located in the GSM x-z-plane.

probable substorm onset latitude and local time. In sunlight, substorm onsets occur 1 hour earlier in local time and 1.5 more poleward than in darkness. The solar wind input, represented by the merging electric field, integrated over 1 hour prior to the substorm, correlates well with the latitude of the breakup. Most poleward latitudes of the onsets were found during very quiet times. Field-aligned and Hall currents observed concurrently with the onset are consistent with the signature of a westward traveling surge evolving out of the Harang discontinuity. The observations suggest that the ionospheric conductivity has an influence on the location of the precipitating energetic electrons, which cause the auroral break-up signature.

For the present report all FUV-images from January 1, 2003 to the end of the IMAGE science mission on December 18, 2005 were analyzed to identify substorm onsets in time and location. The strong orbit precession of IMAGE had moved the apogee across the equator and a large portion of the onsets was observed in the southern hemisphere. That allows for a comparison between the hemispheres. Furthermore, observations between May 2000 and December 2002 cover the peak of the past solar cycle while the present study interval occurred during the declining phase. As in the first publication, the full data set is published electronically and provides a list to the scientific community that can be used for further research.

2. Instrumentation

The IMAGE satellite is in a highly elliptical polar orbit of 1000 x 45600-km altitude with a 14:14 hours orbital period and had the apogee over the North Pole in 2001. The strong precession of $\approx 45^\circ$ per year moved its apogee across the equator in 2003 and down over the South Pole in 2005 (Figure 1).

The Far Ultra-Violet imager (FUV) consists of three imaging sub-instruments and observes the aurora for 5-10 seconds during every 2 minutes spin period [17]. As in the previous report we used the Wideband Imaging Camera (WIC) and the Spectrographic Imager channel (SI-13), and we neglect the proton contribution to the substorm onset aurora [18].

WIC offers the best spatial resolution with a pixel size from apogee of 50 km while the pixel size of SI-13 is 100 km from apogee. During closer proximity the spatial resolution improves but the field of view becomes too small to cover the whole Earth. FUV is turned off during the passage through the radiation belt. That operation scheme limits the observation time to 8-10 hours during each orbit. From apogee around the equator the conditions for auroral observations are unfavorable as aurora appears close to the Earth's limb and the location determination becomes unreliable. That limited the useful time for aurora observations to just a few hours per orbit in 2003/2004.

FUV is mounted on the spinning IMAGE satellite. The pointing within the spin plane is regularly corrected with bright UV stars that cross through the field of view [4]. However the final pointing error in the spin plane can be up to 4 pixels while the one perpendicular to the spin plane can be up to 2 pixels. That amounts to the larger uncertainties for the determination in local time in summer and winter, and in latitude in spring and fall.

3. FUV observations

As in the first study we searched through the FUV data and determined the time and location of substorm onsets. The prime data source were the WIC images because of their better spatial resolution. Some additional SI-13 images were used whenever the WIC high voltage was not turned on or they offered a better view. Substorms were identified if they fulfilled the following criteria:

- A clear local brightening of the aurora has to occur.
- The aurora has to expand to the poleward boundary of the auroral oval and spread azimuthally in local time for at least 20 Minutes.
- A substorm onset was only accepted as a separate event if at least 30 Minutes had passed after the previous onset.

Within the image of the initial auroral brightening the center of the substorm auroral bulge was first determined visually. Then a computer program determined the brightest pixel close to this location and calculated its geographic and geomagnetic locations. The full data set is available electronically at <http://sprg.ssl.berkeley.edu/image/> and other scientists are invited to use the data for their research. The list is given in the same format as in [5]. It contains the date and time of each substorm onset, which FUV instrument was used for the identification (WIC or SI-13), the spacecraft geocentric distance, and the brightness (instrument counts) and location (x/y pixel, geographic and geomagnetic) of the brightest pixel within the onset surge. The list can easily be searched for specific criteria like onsets at high magnetic latitude, late local time, onsets within a certain distance to a particular ground station, or onsets with a small distance to the IMAGE spacecraft promising better spatial resolution.

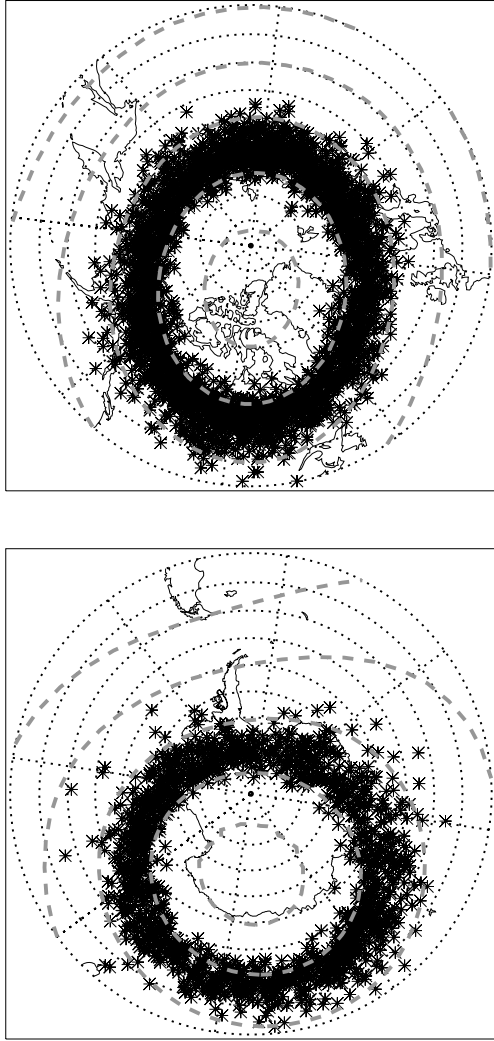


Fig. 2. Maps of the northern (top) and southern (bottom) polar regions with the substorm onset locations in geographic coordinates regardless of the local time of onset. A geomagnetic grid is given as dashed gray lines.

4. Discussion

All onset locations irrespective of their local time are given in Figure 2 separated in the northern and southern hemispheres, respectively. Please note that these plots do not represent the auroral ovals, which are asymmetric between local noon and midnight and move over time in latitude for a fixed longitude (see e.g. [8]). These plots should rather be considered as representations of the auroral zone, statistical maps of the probability for onset observations at a specific geographic location, and maybe as guides to tourists, where to go if you want to see a substorm onset at that particular town/hotel.

The averaged results for the substorm onsets confirm results of earlier studies (Table 1). What is remarkable is the almost perfect reproduction of the locations from the first study with an average MLT of 2250 ± 0127 hours (previously 2300 ± 0121) and latitude of $66.4^\circ \pm 2.96^\circ$ (previously $66.4^\circ \pm 2.86^\circ$) (Figure 3). The match of both parameters is somewhat surprising as other studies found dependences of onset latitudes and local

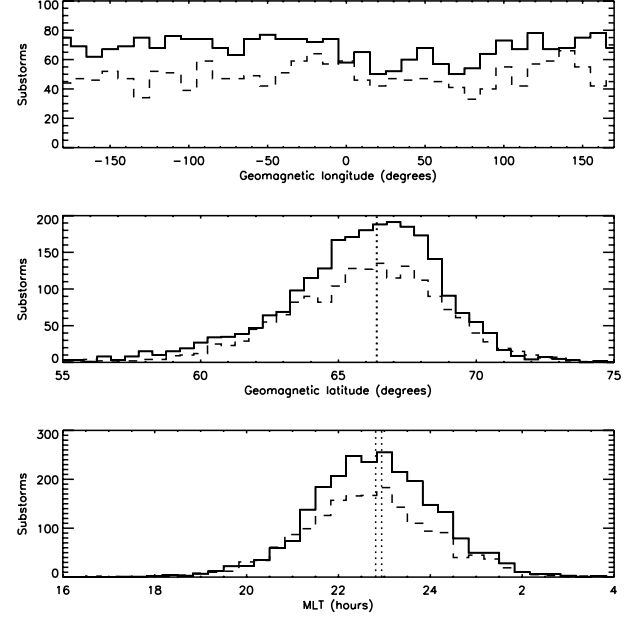


Fig. 3. Histograms of the distribution of substorm onsets in geomagnetic longitude (top), latitude (middle) and local time (bottom) from 2003-2005 (dashed lines) and 2000-2002 (solid lines). The median values are marked in the two bottom panels.

times on the signs of all three IMF components and seasons (see introduction). Especially with respect to the onset latitude, it is not unreasonable to expect some difference between the two data sets as the first one was collected during the peak of the solar cycle and the present one during the declining phase [23]. There are differences between the solar wind properties in the course of the solar cycle. During solar minimum high speed streams are more common [10] and the number of interplanetary coronal mass ejections tracks approximately the sunspot number [12]. That could well influence for instance the onset latitude if these solar cycle changes were for instance accompanied by more negative B_z during solar maximum.

In order to investigate this possibility we analyzed all solar wind plasma and magnetic field measurements by ACE and determined their average properties. Figure 4 summarizes the average IMF conditions for the two time periods from May 2000

Table 1. Median and mean (in parentheses) values of auroral substorm onsets from several statistical studies (from [5]). A large portion of the present onsets was observed in the southern hemisphere and the absolute values of the magnetic latitude were used in the row labeled IMAGE'03.

Satellite	#	MLT (hours)	MLAT (Degrees)	Ref.
DE-1	68	2250 (22.8)	65° (?)	[3]
Viking	133	2305 (22.8)	66.7° (65.8°)	[7]
Polar	648	2230 (22.7)	67° (66.6°)	[11]
IMAGE (winter)	78	2324	65.6°	[6]
IMAGE'00	2437	2300 (23.0)	66.4° (66.1°)	[5]
IMAGE'03 all	1755	2250 (22.8)	66.4° (66.1°)	
IMAGE north	2760	2300 (23.0)	66.3° (66.0°)	
IMAGE south	1432	2245 (22.8)	-66.5° (-66.3°)	

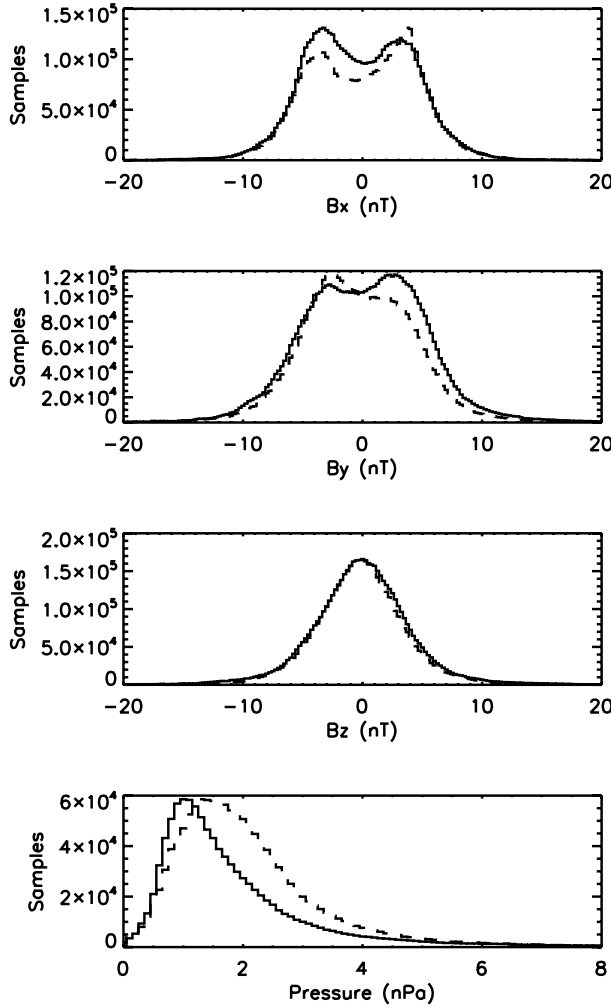


Fig. 4. Histograms of the average IMF conditions as measured by ACE during the two study intervals 2000-2002 (solid lines) and 2003-2005 (dashed lines). Different numbers of measurements were scaled to the maximum of both distributions for easier comparison.

to December 31, 2002 and from January 1, 2003 to December 2005. Accounting for the different numbers of samples in each period we normalized all the distributions to the maximum value in each of the histograms. Table 2 summarizes the median values for the solar wind plasma and magnetic field during these years.

It turns out that the average solar wind properties are not that different between the two time periods. The distributions of GSM- B_z , which could influence the onset latitude, are exactly the same. The distributions of GSM- B_x and B_y are somewhat different. B_x was more negative in 2000-2002 (2.63 Mio. measurements less than 0.0 nT compared to 2.47 Mio. measurements greater than 0.0 nT) than it was in 2003-2005 (2.49 Mio. less than 0.0 nT and 2.77 Mio. greater than 0.0 nT). According to the results in [11] that could have influence on the onset latitude, which we however did not find. The IMF B_y was also slightly different during the two periods. It was more positive in 2000-2002 with 2.68 Mio. measurements with values greater than 0.0 nT compared to 2.42 Mio. measurements

greater than 0.0 nT. This situation was reversed in 2003-2005 when B_y was more negative with 2.80 Mio. measurements less than 0.0 nT and 2.47 Mio. measurements greater than 0.0 nT. In a general sense (see [11]) that should have caused earlier onset local times in 2000-2002 and later onset local times in 2003-2005, what we find neither.

Table 2 also lists the average solar wind plasma conditions during each year of the two periods. However, we only plot the distribution of the solar wind dynamic pressure in Figure 4 as this is the only parameter that was identified as influencing the inset latitude [6]. The two distributions are very different with much larger pressure in 2003-2005 than in 2000-2002. It appears that with a large enough number of events and averages over all seasons, previously established general trends of solar wind influences on the onset locations are suppressed and the magnetosphere creates substorm onsets at constant locations.

5. Summary

The data of the new 1755 substorm onset locations between January 1, 2003 and December 18, 2005 confirm previous findings of average distributions in geomagnetic latitude and local time. The surprising result is the almost perfect match of averaged onset locations that were observed by IMAGE-FUV between 2000 and 2002. The solar wind properties in these two periods at the solar maximum and during the declining phase of the solar cycle were slightly different (B_x and B_y) but these differences were not big enough to change the averaged onset locations substantially. It appears that the average onset locations are more controlled by internal magnetospheric processes than that they are driven by the solar wind.

The prime purpose of this report is to publish the list of FUV substorm observations the same way as it was done in the first investigation. Files summarizing all substorm onsets used for this study are available electronically at the website <http://sprg.ssl.berkeley.edu/image/>. Other researchers are invited to look at those time periods with their data and different instrumentation. The database can easily be searched for specific criteria like onsets at high magnetic latitude, late local time, onsets within a certain distance to a particular ground station, or those with a small distance to the IMAGE spacecraft giving better spatial resolution.

During almost all of the reported substorm onsets there exist also images of the proton aurora taken by the SI-12 channel on IMAGE. Previous analysis of small subsets of FUV images did not find any significant difference in the spatial distribution of the proton and electron onsets [6], but differences in the expansion of the electron and proton precipitation dominated auroras

Table 2. Median values of solar wind plasma and magnetic field properties in the years 2000-2005.

Year	B_x (nT)	B_y (nT)	B_z (nT)	Density (cm $^{-3}$)	Speed (km/s)	Temp. (K)
2000	0.23	0.27	-0.09	4.7	435	68000
2001	-0.17	0.20	0.07	4.5	421	71000
2002	-0.65	0.68	0.10	4.8	439	92000
2003	0.34	-0.41	-0.09	4.1	539	139000
2004	0.79	-0.40	-0.12	4.7	452	92000
2005	-0.05	-0.43	0.01	3.8	501	107000

[18]. Such investigation has not been performed for this study and more statistically significant results could be obtained with a further analysis of the present data set.

Acknowledgments: The IMF and solar wind data were obtained from the ACE Magnetic Field instrument (PI: N. Ness, Bartol Research Institute) and the ACE Solar Wind Experiment (PI: D. J. McComas, Southwest Research Institute). This investigation was supported through subcontract number 03-757 at the University of California at Berkeley under NASA grant NAG5-12762 to the University of New Hampshire.

References

1. Akasofu, S.-I., The development of the auroral substorm, *Planet. Space Sci.*, **12**, 273, 1964.
2. Birn, J., M. Hesse, G. Haerendel, W. Baumjohann, K. Shiokawa, Flow braking and the substorm current wedge, *J. Geophys. Res.*, **104**, 19895, 1999.
3. Craven, J.D. and L.A. Frank, Diagnosis of auroral dynamics using global auroral imaging with emphasis on large-scale evolution, in *Auroral Physics*, ed. C.-I. Meng, M.J. Rycroft, and L.A. Frank, pp. 273-297, Cambridge Univ. Press, New York, 1991.
4. Frey, H.U., S. B. Mende, T.J. Immel, J.-C. Gérard, B. Hubert, S. Habraken, J. Spann, G.R. Gladstone, D.V. Bisikalo, V.I. Shematovich, Summary of quantitative interpretation of IMAGE far ultraviolet auroral data, *Space Science Reviews*, **109**, 255, 2003.
5. Frey, H.U., S.B. Mende, V. Angelopoulos, E.F. Donovan, Substorm onset observations by IMAGE-FUV, *J. Geophys. Res.*, **109**, A10304, doi:10.1029/2004JA010607, 2004.
6. Gérard, J.-C., B. Hubert, A. Grard, M. Meurant, S.B. Mende, Solar wind control of auroral substorm onset locations observed with the IMAGE-FUV imagers, *J. Geophys. Res.*, **109**, A03208, doi:10.1029/2003JA010129, 2004.
7. Henderson, M.G. and J.S. Murphree, Comparison of Viking onset locations with the predictions of the thermal catastrophe model, *J. Geophys. Res.*, **100**, 1857, 1995.
8. Holzworth, R.H. and C.-I. Meng, Mathematical representation of the auroral oval, *Geophys. Res. Lett.*, **2**, 377, 1975.
9. Hones, E.W., Plasma flows in the magnetotail and its implications for substorm theories, in *Dynamics of the Magnetosphere*, ed. S.-I. Akasofu, pp. 545-562, D. Reidel, Norwell, Mass., 1979.
10. Huttunen, K.E.J., R. Schwenn, V. Bothmer, H.E.J. Koskinen, Properties and geoeffectiveness of magnetic clouds in the rising, maximum and early declining phases of solar cycle 23, *Ann Geophys.*, **23**, 625, 2005.
11. Liou, K., P.T. Newell, D.G. Sibeck, C.-I. Meng, M. Brittnacher, and G. Parks, Observation of IMF and seasonal effects in the location of auroral substorm onset, *J. Geophys. Res.*, **106**, 5799, 2001.
12. Liu, Y., J.D. Richardson, and J.W. Belcher, A statistical study of the properties of interplanetary coronal mass ejections from 0.3 to 5.4 AU, *Planet. Space Sci.*, **53**, 3, 2005.
13. Lui A.T.Y., A. Mankofsky, C.-L. Chang, K. Papadopoulos, C.S. Wu, A current disruption mechanism in the neutral sheet: a possible trigger for substorm expansions, *Geophys. Res. Lett.*, **17**, 745, 1990.
14. Lui, A.T.Y., C.-L. Chang, A. Mankofsky, H.-K. Wong, and D. Winske, A cross-field current instability for substorm expansion, *J. Geophys. Res.*, **96**, 11389, 1991.
15. Lyons, L.R., Substorms: Fundamental observational features, distinction from other disturbances, and external triggering, *J. Geophys. Res.*, **101**, 13011, 1996.
16. McPherron, R.L., Substorm related changes in the geomagnetic tail: the growth phase, *Planet. Space Sci.*, **20**, 1521, 1972.
17. Mende, S. B. et al., Far ultraviolet imaging from the IMAGE spacecraft, *Space Sci. Rev.*, **91**, 287, 2000.
18. Mende, S.B., H.U. Frey, B.J. Morsony, and T.J. Immel, Statistical behavior of proton and electron auroras during substorms, *J. Geophys. Res.*, **108**, 1339, doi:10.1029/2002JA009751, 2003.
19. Østgaard, N., S.B. Mende, H.U. Frey, T.J. Immel, L.A. Frank, J.B. Sigwarth, T.J. Stubbs, Interplanetary magnetic field control of the location of substorm onset and auroral features in the conjugate hemispheres, *J. Geophys. Res.*, **109**, A07204, doi:10.1029/2003JA010370, 2004.
20. Parkinson, M.L., M. Pinnock, J.A. Wild, M. Lester, T.K. Yeoman, S.E. Milan, H. Ye, J.C. Devlin, H.U. Frey, and T. Kikuchi, Interhemispheric asymmetries in the occurrence of magnetically conjugate sub-auroral polarization streams, *Ann. Geophys.*, **23**, 1371-1390, 2005
21. Provan, G., M. Lester, S. Mende, and S. Milan, Statistical study of high-latitude plasma flow during magnetospheric substorms, *Ann. Geophys.*, **22**, 3607, 2004.
22. Shiokawa, K., G. Haerendel, W. Baumjohann, Azimuthal pressure gradient as driving force of substorm currents, *Geophys. Res. Lett.*, **25**, 959, 1998.
23. Tanskanen E., T.I. Pulkkinen, H.E.J. Koskinen, J.A. Slavin, Substorm energy budget during low and high solar activity: 1997 and 1999 compared, *J. Geophys. Res.*, **107**, 15-1-11, 2002.
24. Wang, H., H. Lühr, S.Y. Ma, P. Ritter, Statistical study of the substorm onset: its dependence on solar wind parameters and solar illumination, *Ann. Geophys.*, **23**, 2069, 2005.

